Journal of Geophysical Research: Oceans

RESEARCH ARTICLE
10.1029/2018JC014049

The Interannual Variability of the Breakdown of Fall Stratification on the New Jersey Shelf

Jacob Forsyth[1,2], Glen Gawarkiewicz[1], Magdalena Andres[1], and Ke Chen[1]

[1]Department of Physical Oceanography, Woods Hole Oceanographic Institution, Woods Hole, MA, USA, [2]Department of Earth, Atmospheric, and Planetary Sciences, Massachusetts Institute of Technology, Cambridge, MA, USA

Key Points:
- There is large interannual variability in the strength of the shelf's initial fall stratification and in the timing of its destratification
- Wind forcing tends to be one of the most important factors in reducing stratification through 3-D oceanic processes
- Salinity fields play an important role in the fall breakdown of stratification by storms

Correspondence to:
J. Forsyth,
jforsyth@whoi.edu

Citation:
Forsyth, J., Gawarkiewicz, G., Andres, M., & Chen, K. (2018). The interannual variability of the breakdown of fall stratification on the New Jersey shelf. *Journal of Geophysical Research: Oceans*, *123*, 6503–6520. https://doi.org/10.1029/2018JC014049

Received 5 APR 2018
Accepted 20 AUG 2018
Accepted article online 24 AUG 2018
Published online 12 SEP 2018

Abstract During the seasonal evolution of stratification on the New Jersey shelf in the fall, strong thermal stratification that was established in the preceding summer is broken down through wind-driven processes and surface cooling. Ten years of output from a Regional Ocean Modeling Systems run and a one-dimensional mixed layer model is used here to examine the interannual variability in the strength of the stratification and in the processes that reduce stratification in fall. Our analysis shows that the strength of the stratification at the end of the summer is not correlated with the timing of shelf destratification. This indicates that processes that occur within the fall are more important for the timing of stratification breakdown than are the initial fall conditions. Furthermore, wind-driven processes reduce a greater fraction of the stratification in each year than does the surface cooling during the fall. Winds affect the density gradients on the shelf through both changes to the temperature and salinity fields. Processes associated with the downwelling-favorable winds are more effective than those during upwelling-favorable winds in breaking down the vertical density gradients. In the first process, cross-shelf advective fluxes during storms act to decrease stratification during downwelling-favorable winds and increase stratification during upwelling-favorable winds. Second, there is also enhanced velocity shear during downwelling-favorable winds, which allows for more shear instabilities that break down stratification via mixing. Observational data and model output from Tropical Storm Ernesto compare favorably and suggest that downwelling-favorable winds act through the mechanisms identified from the Regional Ocean Modeling Systems results.

Plain Language Summary During summer, the water on the continental shelf off the coast of New Jersey is warm at the surface while capping cold water at the bottom. This temperature difference leads to a large change in density from the surface to bottom, which is known as the seasonal stratification. During fall, this density difference breaks down leading to a well mixed water column in winter. Here we use a 10-year numerical model output to study the processes that break down the stratification in fall, and the variability in how these processes reduce stratification from year to year. Both the strength of the seasonal stratification at the end of summer and the timing when this stratification breaks down during fall is variable from year to year. Wind-driven processes are typically the most responsible for the breakdown of stratification in each year. Strong winds blowing over the ocean lead to processes like mixing and ocean flows. Winds in the northeasterly direction tend to reduce stratification more, as the ocean flows driven by northeasterly winds transport heavier saltier water over lighter fresher water. The processes revealed by the model are also found in the observational data during Tropical Storm Ernesto in 2006.

1. Introduction

Annually averaged ocean temperatures observed off New Jersey on the Middle Atlantic Bight (MAB) shelf show both recent warming at enhanced rates relative to warming trends observed earlier in the record and recent increase in interannual variability (Chen, Gawarkiewicz, et al., 2014; Forsyth et al., 2015; Friedland & Hare, 2007). The accelerated warming of the MAB shelf is also consistent with the enhanced warming trend in sea surface temperature observed in the Gulf of Maine (e.g., Mills et al., 2013; Pershing et al., 2015). Previous work using data from the Oleander Line, an expendable bathythermograph (XBT) repeat line across the New Jersey shelf, suggests that since 1977, the most pronounced warming and the strongest interannual variability manifest in the fall (Forsyth et al., 2015). Fall temperature structure on the MAB shelf directly influences recruitment of commercially important fish species like yellowtail flounder (Sullivan et al., 2005), and the intensity and path of tropical storms that move up the U.S. East Coast (Glenn et al., 2016; Lau et al., 2016).

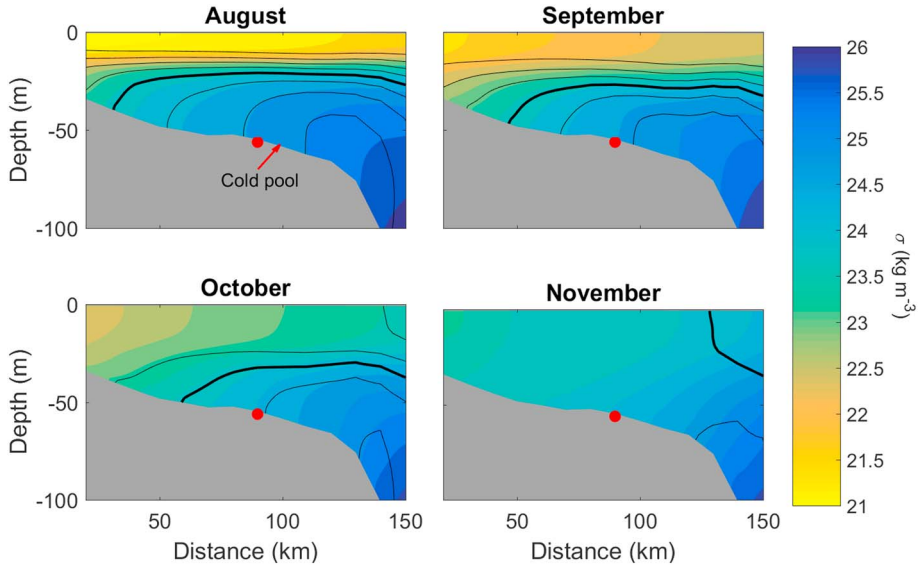

Figure 1. Transects of potential density (colored shading) for different climatological months from the Middle Atlantic Bight and Gulf of Maine model output. The transect shown here is along *Model Transect* from Figure 3. Contours of potential temperature are plotted every 2 °C in black; the bold line marks the 14 °C contour. The red circle is at the 55-m isobath, within the cold pool.

The evolution of the seasonal stratification in fall directly influences the fall temperatures on the MAB continental shelf (Figure 1; Beardsley et al., 1985; Linder & Gawarkiewicz, 1998). During the summer, when atmospheric heating warms the surface water and creates thermal stratification, a strong vertical thermocline separates the warm surface layer from the remnant winter water known as the cold pool (e.g., Houghton et al., 1982; Lentz, 2017). This thermal stratification breaks down during the fall leading to relatively homogenous shelf waters in winter. The breakdown of fall stratification directly determines the thermal structure on the shelf (Figure 1) and thus is important in setting shelf conditions in the following seasons. This also has economic significance as the catches of both squid and lobster have extended later into the fall in some recent years (Hare et al., 2016; Rheuban et al., 2017).

This fall erosion of MAB shelf stratification is thought to result both from increased wind energy available for mixing and from the onset of surface cooling (Beardsley et al., 1985; Mooers et al., 1976). Lentz et al., (2003, hereafter referred to as L03) report on observations from the fall of 1996 on the New England Shelf (northeast of our study area), where wind-driven processes dominated the breakdown of stratification, primarily through high wind events in the downwelling-favorable direction (easterly in L03). Since the observational program in L03 only documented a single fall, how the breakdown in fall stratification varies interannually, including the timing and driving processes, remains an open question. In particular, the relative importance of wind mixing, surface cooling, and three-dimensional oceanic processes is not well quantified from year to year. Considering the recent changes on the MAB shelf and the direct impact of stratification on the shelf conditions and ecosystem, it is both timely and important to understand better the breakdown of stratification in fall.

Here we examine the interannual variability in the relative impacts of both wind and surface cooling on the fall breakdown of stratification using a numerical model simulation from 2004 to 2013 across the New Jersey shelf. We study the New Jersey shelf as a region representative of the southern MAB defined as south of Hudson Canyon, focusing on the dynamics that breakdown stratification over the cold pool. Numerical model hindcasts provide a viable way of examining the problem over a 10-year time span, in contrast to most observational programs in the area that have typically been limited to a single year (i.e., Houghton et al., 1982; Lentz et al., 2003). The model configuration and forcing are described in section 2, together with a description of the data used to evaluate the validity of the model. In section 3 we describe the interannual variability on the New Jersey shelf as represented by the model in terms of (1) initial fall stratification, (2) the date of the initial destratification, and (3) the relative contributions of surface cooling and wind-driven processes. In section 4, we show that downwelling-favorable winds are able to reduce stratification more effectively than upwelling-favorable winds through buoyancy fluxes of both heat and salt, and through enhanced velocity

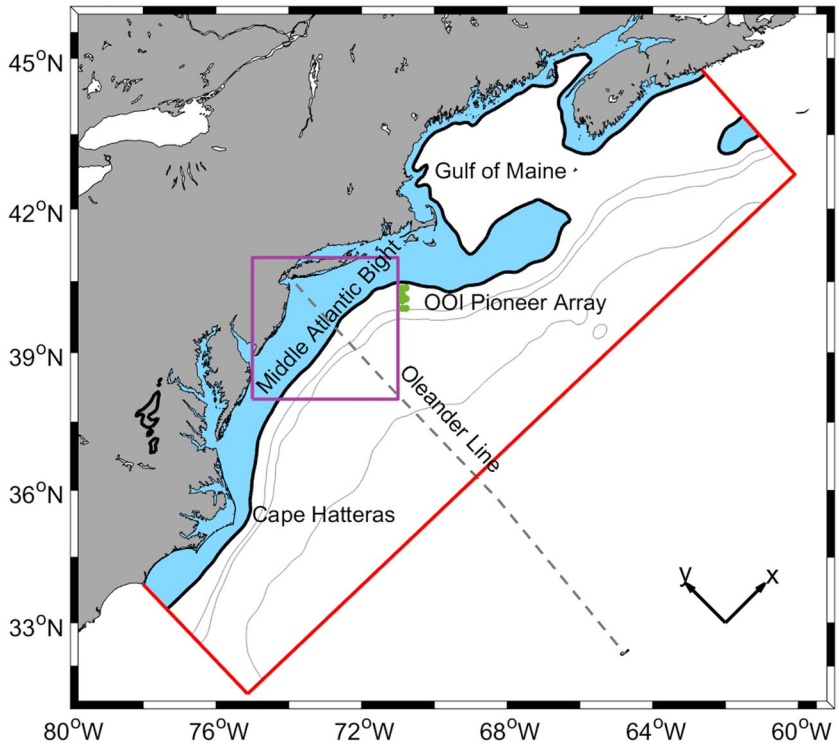

Figure 2. Map of the Middle Atlantic Bight and Gulf of Maine model domain. The continental shelf is highlighted in blue and bounded by the smoothed 80-m isobath (black bold line). The 1,000, 2,000, and 4,000-m isobaths in the model are countoured in gray. The red line marks the boundary of the model. The purple box shows the domain of Figure 3.

shear throughout the water column. Finally, we compare model output and observations from before and after Tropical Storm Ernesto in section 5 in order to qualitatively confirm that three-dimensional processes are important in the breakdown of stratification. Conclusions appear in section 6.

2. Methodology

We use two complementary modeling approaches to examine the breakdown of stratification in the fall. First, we examine the output from a regional general circulation model, driven by realistic oceanic and atmospheric forcings. Then we use a one-dimensional mixed layer model to elucidate the roles of wind forcing and buoyancy forcing during the stratification breakdown. Despite differences between the model's mixing schemes, this approach helps clarify some of the contributions of three-dimensional processes by comparing the regional model output to the output from the one-dimensional model run with the various forcing terms.

2.1. The Regional Circulation Model

We use existing model output from a regional general circulation model (MAB and Gulf of Maine, MABGOM) described by Chen and He (2015) and Chen, He, et al. (2014). Here we only describe important details of the model that are relevant to this study.

The model is the hydrostatic Regional Ocean Modeling System configured for the Northwest Atlantic continental shelf region. The Regional Ocean Modeling System is a free-surface, primitive-equation model mapped onto vertically stretched, terrain-following coordinates using algorithms described by Shchepetkin and McWilliams (2005) and Haidvogel et al. (2008). Vertical turbulent mixing is calculated following the methodology of Mellor and Yamada (1982). Quadratic bottom drag is used with a drag coefficient of 0.003. The domain of the model extends from Cape Hatteras to Nova Scotia (Figure 2) covering the MAB and the Gulf of Maine. Horizontal resolution is 10 km in the along-shelf direction and 6 km in the cross-shelf direction. There are 36 vertical bins which are higher resolution near the surface and bottom in order to more accurately resolve the boundary layers.

The model's initial and boundary conditions are derived from the 1/12° daily mean fields from the Hybrid Coordinate Ocean Model Naval Research Laboratory Coupled Ocean Data Assimilation (HYCOM/NCODA)

output (Chassignet et al., 2007). The lack of coastal processes (e.g., river outflows and tidal mixing) in the HYCOM/NCODA leads to temperature and salinity biases that are strongest on the continental shelf. To correct for these biases, the HYCOM annual mean salinity and temperature fields are replaced with the HydroBase Hydrographic climatological field for each given year (Curry, 1996). Dynamic height and geostrophic transport are also adjusted to be consistent with the corrected temperature and salinity fields. This correction removes the annual mean biases, but maintains the daily variability of the HYCOM/NCODA output.

Surface forcing comes from the North America Regional Reanalysis (NARR) provided by National Oceanographic and Atmospheric Administration (NOAA) National Centers for Environmental Prediction. This product has a 35-km spatial resolution and 3-hr temporal resolution. Surface buoyancy and momentum fluxes are calculated using the standard bulk formulae (Fairall et al., 2003). The surface net heat fluxes are additionally adjusted through a thermal relaxation term based on the daily blended cloud-free surface temperature field produced by NOAA Ocean Watch, with an adjustment time scale of 12 hr (e.g., Chen & He, 2015).

The model hindcast begins on 1 November 2003 using the corrected HYCOM/NCODA fields and is run until 31 December 2013, providing 10 years of model output from 2004 to 2013. Model output is averaged over the M_2 tidal cycle providing a temporal resolution of 12.42 hr.

We extract a cross-shelf transect from the model with $x > 0$ in the northeast (i.e., along-shelf) direction and $y > 0$ in the northwest (i.e., cross-shelf) direction (Figure 2). The transect is chosen to coincide with the Oleander Line along which data are collected by the CMV *Oleander*. The CMV *Oleander* is a NOAA Ship of Opportunity scientific sampling platform that has been in operation since 1977 taking measurements which include profiles of temperature and velocity, and surface salinity (Flagg et al., 2006). For the purpose of analysis, we focus here on the point where the 55-m isobath intersects this transect to study the breakdown of stratification over the cold pool (Forsyth et al., 2015; Linder & Gawarkiewicz, 1998). Focusing on the 55-m isobath also minimizes any influence of the position of the model's meandering shelfbreak front. The shelfbreak front in this area of the MAB has a mean grounding position at the 80-m isobath (Fratantoni & Pickart, 2007), with typical meanders of 10–20 km in the cross-isobath direction (Boicourt & Hacker, 1976). A large-amplitude meander was previously observed to have a cross-isobath amplitude of approximately 30 km, which would reach the 60-m isobath on this transect (Gawarkiewicz et al., 2004). Using the 55-m isobath allows us to examine the processes which influence stratification in the fall without having to consider movements of the shelfbreak front.

2.2. The One-Dimensional Model

A one-dimensional mixed layer model (PWP model; Price et al., 1986) is also used to isolate the impact of individual surface fluxes. The PWP model considers 1-D water column instability and mixing in response to surface heat, freshwater, and momentum fluxes. The model is initialized with a temperature/salinity profile and steps forward in time forced with seven real-time atmospheric variables including turbulent (latent and sensible) and radiative (shortwave and longwave) fluxes, vector (eastward and northward) wind stress, and precipitation rate. At each time step, the fluxes are applied to the top layer of the water column except for shortwave radiation, which is distributed over multiple layers using a distribution profile based on Paulson and Simpson (1977). The water column then mixes from surface to depth to eliminate static instability. The model further considers entrainment below the initial mixed layer according to the Bulk Richardson Number criterion (critical value 0.65). In addition, the PWP model also considers instability below the mixed layer by ensuring Gradient Richardson Number (R_g) greater than a critical value (0.25).

We run the PWP model from 1 August to 31 December of each year from 2004 to 2013. In each year, MABGOM output is used to initialize the PWP model. The year's initial water column in PWP is taken from the 1–14 August mean of MABGOM temperature, salinity, and velocity profiles at the 55-m isobath (Figure 3). Surface heat fluxes and buoyancy fluxes are taken from the 3-hourly NARR product. Momentum fluxes are calculated from winds speed at 10 m from the NARR, using the bulk methodology of Large and Pond (1981).

Three different forcing scenarios are used here for the PWP model. The first run, PWP ALL, uses heat, freshwater, and momentum fluxes as specified above. We also run the mixed layer model with the heat fluxes in isolation which will be called PWP HEAT. Third, we run the mixed layer model with only the momentum fluxes due to wind forcing which is abbreviated as PWP WIND.

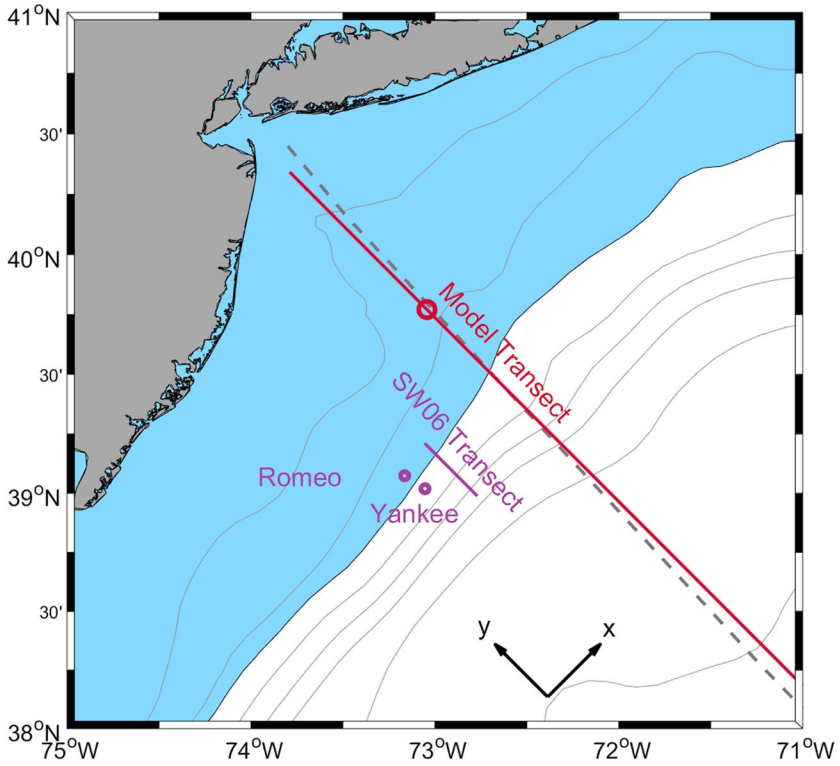

Figure 3. A zoomed in section of Figure 2 (marked as the purple box). Here we also identify the model transect along which output is extracted (red line) and the 55-m isobath on this transect (red circle). The Shallow Water '06 mapped transect is plotted as a purple line with the two Air-Sea Interaction Spar buoys, Romeo and Yankee, plotted as purple circles.

2.3. Shallow Water '06

The MABGOM model has been tested and validated in previous work (Chen & He, 2015). To further assess the model in simulating the effect storms have on stratification, we utilize observational data from the Shallow Water '06 (SW06) experiment, a large-scale experiment off the coast of New Jersey in summer 2006 (Tang et al., 2007). During the experiment, Tropical Storm Ernesto passed through the study area at the end of August overlapping with both shipboard and mooring measurements. The observations from the storm are used to examine the cross-shelf advective processes in the MABGOM model fields with the observations.

For this study, we use a combination of the mapped shipboard measurements of temperature and salinity from Scanfish surveys, and mooring observations of wind data from the two Air-Sea Interaction Spar buoys, Romeo and Yankee (Figure 3), deployed by H. Graber of the University of Miami. The shipboard measurements included a total of 12 surveys, each consisting of four to eight cross-shelf and along-shelf transects, occupied between 25 August and 9 September. Potential temperature and salinity fields were interpolated onto a mapped grid with horizontal resolution of 0.02 km and vertical resolution of 2 m (Tang et al., 2007). We extract a cross-shelf transect through this mapped grid for each survey. The final transect used, along with the mooring locations can be seen in Figure 3. Surveys from 25 August to 30 August were sampled before the tropical storm and are used in the analysis in section 5, while surveys after the tropical storm from 3 to 9 September (Figure 14) are used to examine the stratification after the storm. The comparison between the prestorm and poststorm transects allows for examination of the spatial pattern of the changes in stratification and, as will be seen, the verification of the importance of cross-shelf Ekman buoyancy flux. Wind speed and wind direction were measured by the Air-Sea Interaction Spar buoys and provided as hourly averages. The winds are rotated onto along-shelf and cross-shelf components consistent with the orientation of the transect (x and y in Figure 3). These winds were then box averaged over a 12-hr interval to emulate the model output.

For comparisons between the model and the observational data, we extracted model fields from the same days and same locations as SW06 for the shipboard measurements and the same times and a position between the two moorings for the meteorological data. Comparing model forcing with the meteorological data allows

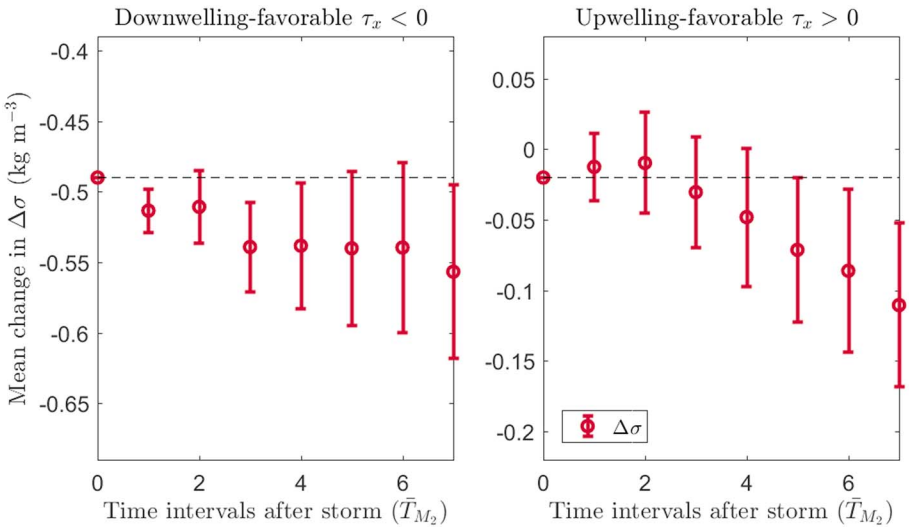

Figure 4. The mean change of $\Delta\sigma$ as a function of the number of Middle Atlantic Bight and Gulf of Maine model time intervals after a storm is over with standard errors plotted as error bars. The means are only calculated for storms that did not have another storm within the restratification period considered (eight time intervals of 12.42 hr after a storm has ended). Left panel only considers downwelling-favorable storms, and the right panel only considers upwelling-favorable storms. Black dashed line shows the mean change in stratification by the storms considered. Both *y* axes span the same range. Negative values represent destratification.

us to estimate the accuracy of the atmospheric forcing used. Qualitative similarities in the potential temperature and salinity fields provide evidence of the influence of cross-shelf advective processes. Differences between the model and data are likely due to additional processes like the warm core ring found in the observations.

2.4. Defining Stratification

In order to quantify stratification on the shelf and examine its temporal evolution in fall, we calculate a vertical density difference, $\Delta\sigma$, at each model time interval. $\Delta\sigma$ is the difference between the near-surface potential density and near-bottom potential density, where near-surface and near-bottom values are calculated from vertically averaging the uppermost and bottommost 7.5 m of the water column respectively, consistent with the methodology of L03. The top 7.5 m of the water column is always within the mixed layer for all time points considered in this study. To examine separately the roles of temperature and salinity in setting and eroding stratification on the shelf, we define the contribution to $\Delta\sigma$ of potential temperature ($\Delta\sigma_\theta$) and salinity ($\Delta\sigma_S$) using a linear equation of state where

$$\begin{aligned} \Delta\sigma_\theta &= -\alpha\rho_{\text{ref}}((\theta_{\text{bot}} - \theta_{\text{surf}})), \\ \Delta\sigma_S &= \beta\rho_{\text{ref}}((S_{\text{bot}} - S_{\text{surf}})). \end{aligned} \tag{1}$$

Here we denote potential temperature as θ, salinity as S, and density as ρ. Reference values of θ, S, and ρ are mean values on the New Jersey shelf in the fall, which are $\theta_{\text{ref}} = 15.5\ ^\circ\text{C}^{-1}$, $S_{\text{ref}} = 32$, and $\rho_{\text{ref}} = 1{,}025\ \text{kg/m}^3$. For this study we use α, the thermal expansion coefficient, as $2\times10^{-4}\ ^\circ\text{C}^{-1}$ and β, the haline contraction coefficient, as 7.5×10^{-4}, which are calculated from the reference values. Note that the MABGOM model does not use a linear equation of state, but we implement the definitions in equation (1) as a way of isolating the effects of temperature and salinity.

To calculate each year's initial fall stratification, we temporally average potential temperature and salinity profiles from 1 August to 14 August of a given year. We define the destratification point as the first time period (after mid-August) during which $\Delta\sigma \leq 0.5\ \text{kg/m}^{-3}$. This definition is used so that all time points considered in this study have existing stratification which can be reduced or increased. After this destratifiaction point, restratifcation events may occur; however, these events are always small relative to the initial fall stratification at the end of summer (Figure 4). Our results are not sensitive to the $\Delta\sigma$ value chosen to define the destratification point.

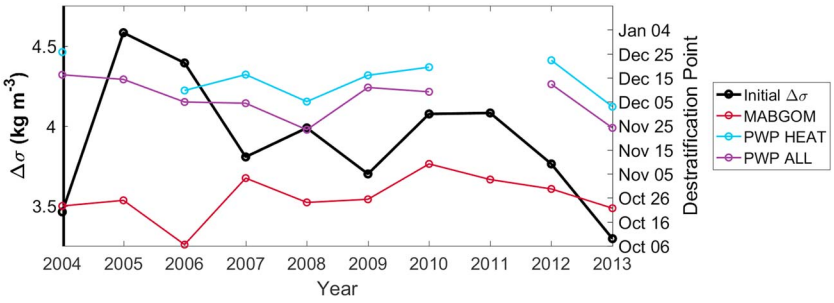

Figure 5. Interannual variability of the initial fall stratification from the MABGOM model (thick black line associated with the left *y* axis) and the interannual variability of the destratification point (right *y* axis) for the MABGOM model (red), the PWP HEAT (blue), and PWP ALL (purple). PWP WIND never reaches the destratification point by the end of each year and thus is not shown. MABGOM = Middle Atlantic Bight and Gulf of Maine.

It will be confirmed here that storms impact the stratification on the continental shelf through both high wind stresses and strong heat fluxes. Throughout the 10 years examined in the models, 63 storms occur during the fall while the water column is stratified. We define storms following the methodology of L03 and consider all time periods where the average wind stress magnitude, τ, is greater than 0.14 N/m^2 as storms. Additionally, anomalous heat fluxes that occur in time intervals adjacent to times of high wind stress are defined as part of the same storm event. Anomalous heat fluxes are defined based on the net surface heat flux output from the model. The net surface heat flux from the model is diurnally averaged (over M_2 tidal cycle, 12.42 hr), and then linearly detrended from 1 August to 31 December of each year. We consider a heat flux as anomalous if it is over two standard deviations from the diurnally averaged linearly detrended output.

In order to calculate the net effects of an individual storm's heat flux and wind stress on stratification, we calculate the change in our stratification parameters ($\Delta\sigma$, $\Delta\sigma_\theta$, and $\Delta\sigma_S$) from the time interval before the storm began and the time interval after the storm has ended (keeping in mind that the time intervals are 12.42 hr). Storms beginning later in the year after the destratification point are not considered. Furthermore, if stratification is reduced to less than 0.5 kg/m^3 during an identified storm event, we only consider the effect of the storm up until the destratification point.

3. Interannual Variability of the Breakdown of Stratification

On average, initial fall stratification on the New Jersey shelf is 3.9 kg/m^3 over 2004–2013 (Figure 5). Stratification at the start of August ranges from a minimum of 3.3 kg/m^3 in 2013 to a maximum of 4.6 kg/m^3 in 2005. Typically, temperature plays an important role in setting the initial shelf stratification as the contribution of thermal stratification ($\Delta\sigma_\theta$) constitutes 80% of the initial fall stratification ($\Delta\sigma$), which is consistent with previous research on the MAB (Li et al., 2015).

The destratification point simulated here varies strongly across the four different model runs (MABGOM, the regional general circulation model; PWP ALL, one-dimension mixed layer model with heat, freshwater, and momentum fluxes; PWP HEAT, one-dimension mixed layer model with only heat fluxes; and PWP WIND, one-dimension mixed layer model with only momentum fluxes) and from one year to the next within each model (Figure 5). The shelf water column typically first destratifies by late October in the MABGOM model, but the destratification point ranges from early October to early November in different years. Of the four model runs, the shelf water column in the three-dimensional MABGOM model always reaches the destratification point at least 2 months before that modeled with any of the one-dimensional PWP simulations and none of the PWP runs consistently reaches a destratified state by 31 December in every year. For the PWP simulations, ALL and HEAT destratify at a similar date. This suggests that it is the heat fluxes rather than momentum fluxes that drive the destratification in the one-dimensional cases.

However, the more rapid destratification in the MABGOM simulation compared to the PWP simulations suggests that three-dimensional processes play an important role in eroding the stratification on the New Jersey shelf. Specifically, the role of the Ekman buoyancy fluxes in reducing stratification is significant and is described in further detail in section 4. Somewhat counterintuitively, over the 10-year period simulated by the MABGOM model, each year's initial fall stratification is not significantly correlated with that year's

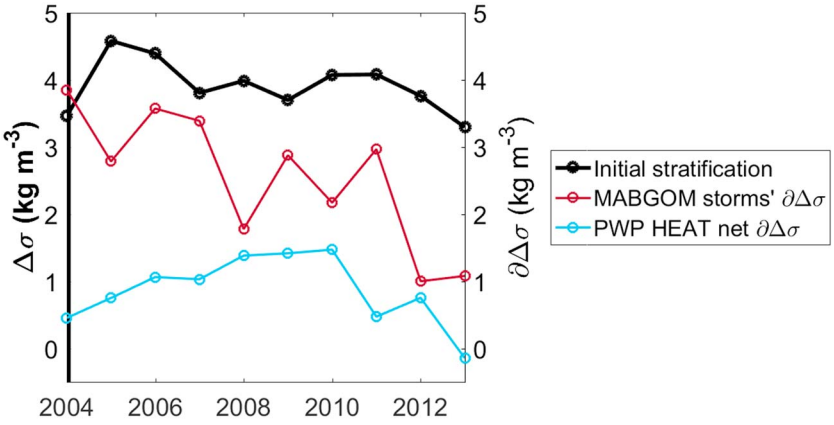

Figure 6. Interannual variability of the initial fall stratification from the MABGOM model (thick black line associated with the left *y* axis) and the interannual variability of how storms in the MABGOM model impact stratification (red) and how heat fluxes (PWP HEAT) impact stratification (teal). For PWP HEAT the net change in $\Delta\sigma$ from initial fall stratification until the destratification point as defined from the MABGOM model is plotted. MABGOM = Middle Atlantic Bight and Gulf of Maine.

destratification point. This lack of correlation implies that it is the forcing that occurs within each fall (rather than the initial conditions at the beginning of fall) that determine when the shelf is destratified.

Previous work has suggested that surface cooling and increased wind stress are both important mechanisms that reduce stratification during fall (Beardsley et al., 1985; Houghton et al., 1982). Their relative importance and the roles of temperature versus salinity in the destratification processes are examined here by comparing output from the various model runs. We first determine for each year the destratification point in the MABGOM model. With this date, we then calculate the change in stratification as modeled with the PWP HEAT run, starting with the initial fall stratification and ending with the PWP HEAT model's stratification on this (MABGOM model derived) date. This isolates the impact that heat fluxes alone have in reducing stratification (Figure 6). Considering all years together, heat fluxes alone reduced the initial fall stratification by 20%. The interannual variability in the influence of heat flux in eroding initial fall stratification varies from a 38% reduction in 2009 to actually increasing initial fall stratification by 5% in 2013. Despite this strong interannual variability in the effect of heat flux on stratification, the heat flux generally tends to reduce only a small fraction of the initial stratification. Finally, this calculated impact of the heat fluxes on the reduction of stratification is not correlated with the date of the end of stratification.

With this limited influence of heat flux on the erosion of stratification established, we further investigate the impact that fall storms have on the stratification by summing within each year the stratification change from each individual storm and comparing this across models. Fall storms in the MABGOM model reduce stratification by a greater amount than do total heat fluxes alone from the PWP HEAT experiment (Figure 6). The net reduction in stratification from storms varies between eroding more than 100% of the initial fall stratification (2004) to eroding around 33% of the initial fall stratification (2012). Storms are able to reduce the initial fall stratification by more than 100% due to restratification events that can occur throughout the fall such as surface heating or advective processes. These restratification events are not connected to storms, as stratification tends to be eroded in the time following a storm event (Figure 4). Overall, storm events appear to be more important in reducing stratification than the seasonal surface cooling, as found in L03.

Storms in each of the one-dimensional model runs also reduce significantly less stratification than do storms in the MABGOM model. Comparisons between simulations using Mellor-Yamada and PWP mixing schemes have shown that both mixing schemes yield similar results in simulating the mixed layer, suggesting that the differences between our two simulations are in large part due to three-dimensional oceanic effects (Halliwell, 2004). As storms (rather than the seasonal cycle of heat flux) appear to be the most important factor in reducing stratification on the New Jersey shelf, and three-dimensional effects are important in reducing stratification, we next consider the processes by which storms can reduce stratification.

Storms can be differentiated by wind direction; that is, those with winds that are predominately upwelling favorable ($\tau_x > 0$, southwesterly) and those with winds that are predominately downwelling favorable ($\tau_x < 0$,

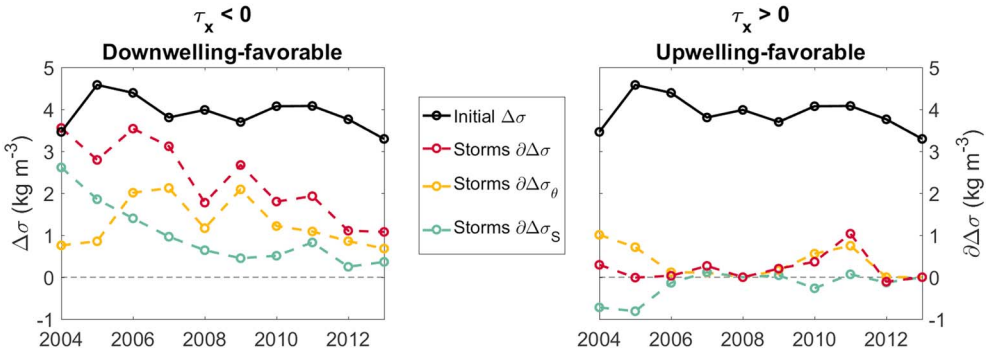

Figure 7. Interannual variability of the initial fall stratification from the MABGOM model (thick black line associated with the left *y* axis) and the interannual variability of the impact of storms in the MABGOM model on overall stratification (red), stratification due to potential temperature (yellow), and stratification due to salinity (green). Left panel is the net effect of downwelling-favorable storms each year, and the right panel is the net effect of upwelling-favorable storms each year. MABGOM = Middle Atlantic Bight and Gulf of Maine.

northeasterly). Differentiating storms this way shows that it is the downwelling-favorable winds that are consistently more effective at reducing stratification (Figure 7). Downwelling-favorable winds are also more common than upwelling-favorable winds; however, even when normalizing the change in stratification for accumulated along-shelf wind stress (the integral of the along-shelf wind stress times duration of each storm), downwelling-favorable winds are still more effective at reducing stratification than are upwelling-favorable winds (Csanady, 1982).

Stratification is reduced after both downwelling-favorable and upwelling-favorable storms (Figure 4). The change in stratification following storm events is significantly correlated to the along-shelf wind stress. In the first two tidal cycles after a storm, the along-shelf winds tend to be in the same direction as they were during the storm event, which results in an increase of stratification after an upwelling-favorable storm, and a decrease in stratification after a downwelling-favorable storm. However, beyond two tidal cycles after a storm event is over, the along-shelf winds tend to reverse direction leading to predominately downwelling-favorable winds after upwelling-favorable storm events and upwelling-favorable winds after downwelling-favorable storms. As the winds reverse in direction, the stratification is reduced more after an upwelling-favorable storm due to downwelling-favorable winds.

Over the 10 years hindcast by the MABGOM model, downwelling-favorable storms tend to reduce less stratification in the later years of the model run. The amount of stratification reduced by storms is strongly correlated with the accumulated along-shelf wind stress only for downwelling-favorable storms (Figure 8). Accumulated along-shelf wind stress is not correlated to the number of storms within a year nor the destratification point, suggesting that the ability for storms to reduce stratification is due to strong individual events

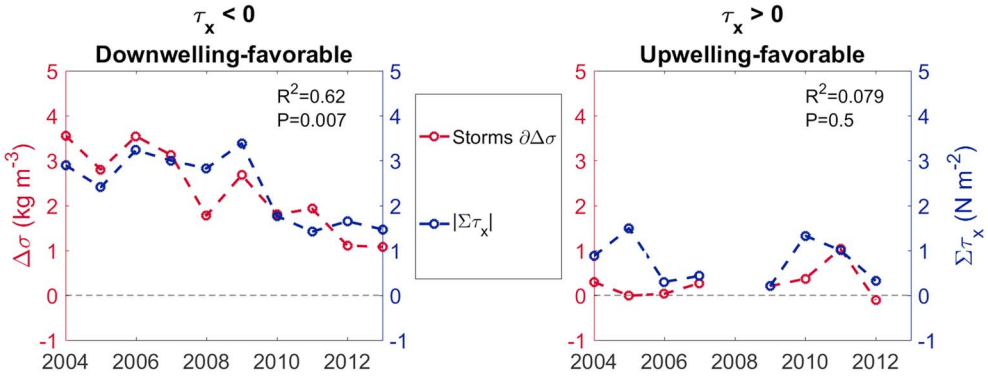

Figure 8. Interannual variability of the impact of storms in the MABGOM model on overall stratification (red), and the accumulated along-shelf wind stress during the storms in the MABGOM model (blue). Left panel is the net effect of downwelling-favorable storms each year, and the right panel is the net effect of upwelling-favorable storms each year. MABGOM = Middle Atlantic Bight and Gulf of Maine.

which vary in frequency and intensity from year to year. In windier years, like that during the observational program described in L03, it would be expected that storms would reduce more stratification than other processes would.

During storms with downwelling-favorable winds, both the thermal and haline stratification are reduced, but the reduction in thermal stratification is typically greater than the reduction in haline stratification (Figure 7). The exceptions are 2004 and 2005 when the downwelling-favorable storms did erode stratification more through changes in the salinity profiles rather than through changes in the temperature profiles. This difference in 2004 and 2005 cannot be explained through the wind since other years with similar accumulated wind stress values reduced stratification primarily through thermal changes. Instead, 55% of the interannual variability in the reduction of stratification due to salinity in downwelling-favorable storms can be explained by the interannual variability in the mean fall cross-shelf salinity gradient (gradients here calculated over a 20-km distance). Years 2004 and 2005 have the strongest cross-shelf salinity gradient and also the greatest change in stratification due to haline changes, while 2012 has the weakest cross-shelf salinity gradient and the least reduction in stratification due to salinity changes.

In contrast, during upwelling-favorable winds, stratification does not tend to change except in 2011, which is driven by the strongest upwelling-favorable storm in the 10 years studied. Interestingly, changes to the salinity structure during upwelling-favorable winds tend to either increase the stratification, or not change the stratification appreciably. The physical mechanisms that connect the winds, cross-shelf gradients, and the change in stratification will be examined in section 4.

To account for the greater frequency of downwelling-favorable winds, we normalize the change in stratification by accumulated wind stress for each storm. The median change in the haline stratification per unit wind stress per unit time (unit time is the model output time interval of 12.42 hr) for downwelling-favorable wind storms and upwelling-favorable wind storms is $-0.35\ \frac{\mathrm{kgm^{-3}}}{\mathrm{Nm^{-2}}\bar{\tau}_{M_2}}$ and $0.21\ \frac{\mathrm{kgm^{-3}}}{\mathrm{Nm^{-2}}\bar{\tau}_{M_2}}$, respectively. Reporting the same numbers but for thermal stratification gives $-0.53\ \frac{\mathrm{kgm^{-3}}}{\mathrm{Nm^{-2}}\bar{\tau}_{M_2}}$ and $-0.28\ \frac{\mathrm{kgm^{-3}}}{\mathrm{Nm^{-2}}\bar{\tau}_{M_2}}$ and for total stratification gives $-0.96\ \frac{\mathrm{kgm^{-3}}}{\mathrm{Nm^{-2}}\bar{\tau}_{M_2}}$ and $-0.15\ \frac{\mathrm{kgm^{-3}}}{\mathrm{Nm^{-2}}\bar{\tau}_{M_2}}$. Normalizing the changes in stratification by the accumulated wind stress shows that downwelling-favorable storms are able to reduce stratification more effectively than upwelling-favorable storms because of both changes to the thermal and haline stratification. A similar conclusion was found in L03 from observations south of New England where only strong downwelling-favorable winds significantly reduced stratification. L03 attributed this to an Ekman buoyancy flux, and a changing along-shelf thermal-wind shear. The use of the MABGOM model here allows for more direct calculations in order to examine what processes lead to the enhanced reduction of stratification by downwelling-favorable winds over multiple years as considered next.

4. Physical Mechanisms Contributing to the Breakdown in Stratification

L03 proposed two mechanisms that can cause downwelling-favorable winds to reduce stratification more effectively than upwelling-favorable winds. The first is an Ekman buoyancy flux, where negative along-shelf wind stress leads to an onshore Ekman transport in the surface layer and an offshore transport in the bottom boundary layer (Straneo et al., 2002). On the New Jersey shelf, there is a mean cross-shelf salinity gradient with fresher waters in the onshore direction (Manning, 1991). Hence, onshore Ekman velocities in the surface layer transport saltier waters onshore and fresher waters offshore at depth which reduces the vertical density gradient. When the Ekman velocities are in the opposite direction, the vertical density gradient is increased (i.e., during upwelling-favorable winds).

The other postulated mechanism discussed by L03 is due to the increased along-shelf vertical shear of the velocities that occurs during downwelling-favorable winds due to an enhanced background thermal-wind shear associated with tilting of the isopycnals. On the MAB outer shelf, the mean thermal-wind shear causes the equatorward along-shelf velocities to decrease with depth. If the Ekman transports act as described above, along-shelf winds would steepen the isopycnals which would increase the cross-shelf density gradient and thus enhance the surface to bottom along-shelf velocity shear. Enhanced velocity shear may allow for more shear instabilities to mix the water column thereby decreasing the stratification.

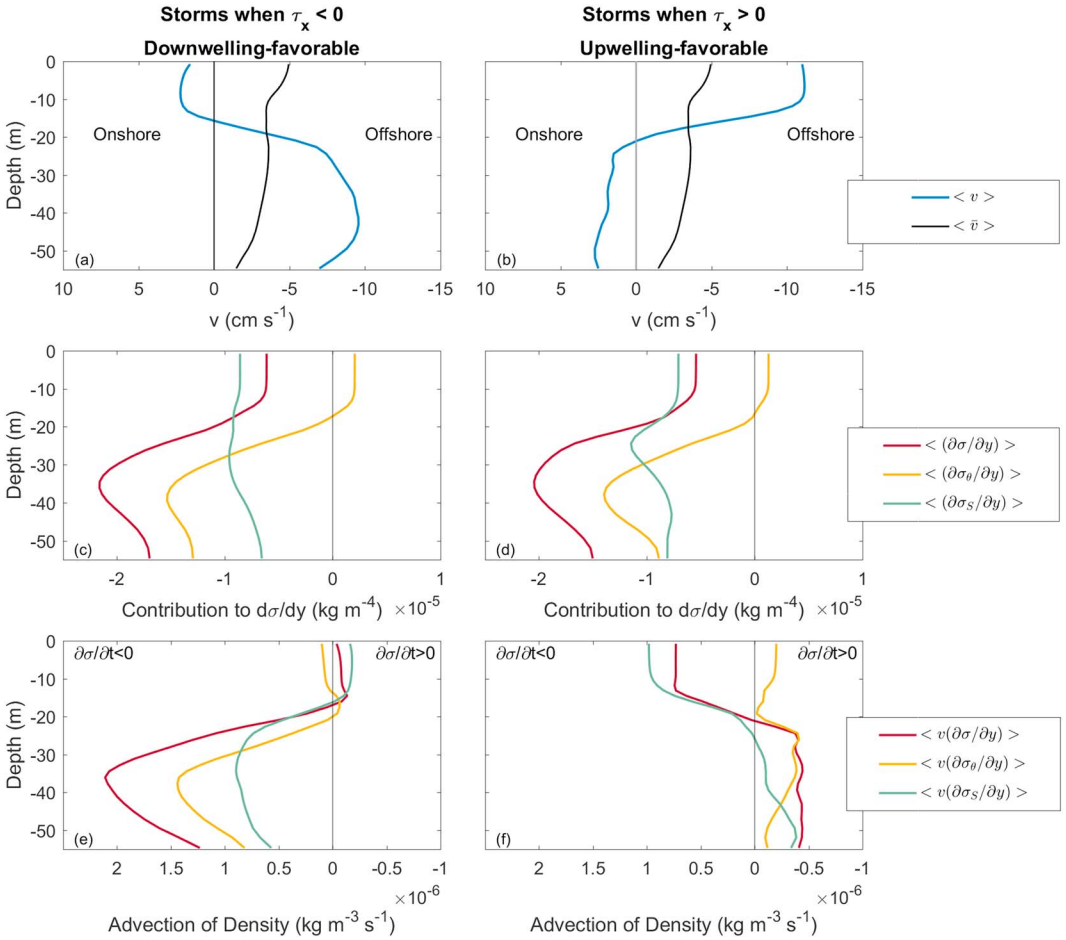

Figure 9. Mean cross-shelf gradients and mean velocities for storms when $\tau_x < 0$ (left column) and $\tau_x > 0$ (right column). (a, b) Mean cross-shelf velocity at the 55-m isobath (blue) during storms. The black line is the mean cross-shelf velocity during the fall. Positive velocities denote onshore transport and negative velocities denote offshore transport. (c, d) Cross-shelf gradients in potential density (red), salinity's contribution to potential density (green), and potential temperature's contribution to potential density (yellow). (e, f) Mean cross-shelf velocity during storms (a, b) multiplied by the cross-shelf gradients (c, d) with colors corresponding to the gradients above (c, d). Negative values are increasing density, and positive values are decreasing density.

4.1. Ekman Buoyancy Flux

To determine if the first mechanism, associated with the Ekman buoyancy flux, is a significant factor in reducing stratification during storms, we examine the mean cross-shelf velocities and mean cross-shelf gradients in $\Delta\sigma$, $\Delta\sigma_\theta$, and $\Delta\sigma_S$ during storms distinguishing between those with downwelling-favorable winds and those with upwelling-favorable winds (Figure 9). The surface Ekman layer is obvious in the model output, with mean surface cross-shelf velocities flowing to the right of the along-shelf winds (Figures 9a and 9b). The average surface velocities for both wind directions (blue curves) deviate by around 7.5 cm/s from the mean fall cross-shelf velocity (black curves). At depth, there is a reversal of the cross-shelf velocity for both wind directions with a large vertical shear between 15 and 25 m.

The mean cross-shelf density gradients are similar during both downwelling- and upwelling-favorable storms as the initial conditions are not dependent on the wind direction (Figures 9c and 9d). During the fall, the cross-shelf variations of temperature within the surface mixed layer are generally weak, while at depth, the cross-shelf variation in temperature is determined by the characteristics of the cold pool (Figure 1). At the 55-m isobath, the cross-shelf gradients in temperature indicate warmer water in the onshore direction, but this gradient is of opposite sign on the offshore side of the cold pool. In this region of the New Jersey shelf, the cross-shelf salinity gradient is negative onshore, that is, salinity decreases shoreward, and is fairly

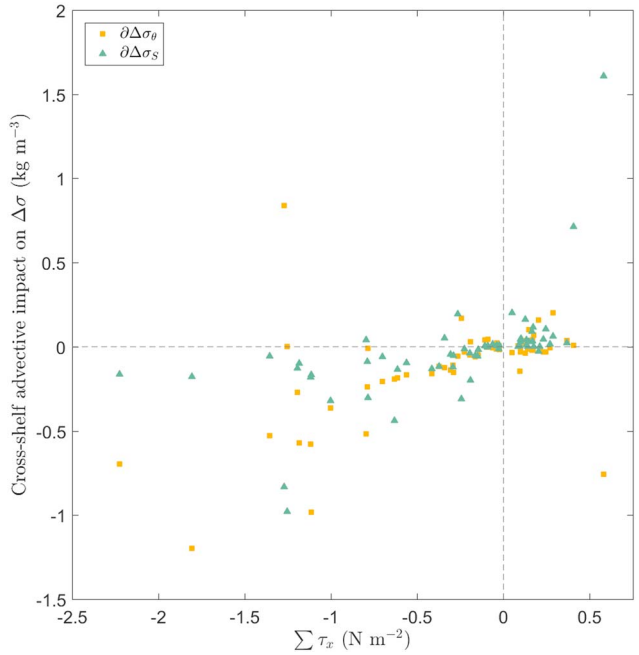

Figure 10. Accumulated along-shelf wind stress (the sum of the average along-shelf wind stress in each time interval during each storm) versus the cross-shelf advective impact on the change in stratification due to changes in potential temperature (yellow squares) and salinity (green triangles) during each storm.

uniform throughout the water column. Thus, in fall on the New Jersey shelf, the cross-shelf density gradient is dependent on both temperature and salinity gradients.

Multiplying the mean cross-shelf velocities with the mean cross-shelf densities for each storm gives the Ekman buoyancy fluxes. These fluxes are then composite averaged for storms characterized by each of the two along-shelf wind directions (Figures 9e and 9f). The net effect of the Ekman buoyancy flux during storms is to reduce stratification for downwelling-favorable winds and to increase stratification for upwelling-favorable winds. Due to the differences between the cross-shelf temperature and salinity gradients, the transport of salt dominates the change in density at the surface, while both the transport of heat and salt impact the change of density near the bottom (Figures 9c and 9d).

During downwelling-favorable storms, cross-shore velocities are weak at the surface but strong at depth, thereby causing both temperature and salinity transports to be important to the density changes over the water column. The cross-shelf salt flux leads to saltier waters moved onshore at the surface and fresher waters moved offshore at depth causing a mean reduction in stratification by 0.13 kg/m^3 (Figure 10). Transport of warmer waters into the cold pool during downwelling-favorable winds also reduces the stratification with a mean reduction of 0.17 kg/m^3 (Figure 10). The mean reduction in stratification by a downwelling-favorable storm is 0.60 kg/m^3, which suggests that cross-shelf buoyancy fluxes are responsible for around half of the change in stratification during storms (Figure 11). These mean values are skewed by a few very strong storms. Calculations using median values instead for downwelling-favorable storms show that the salt flux reduces stratification by 0.06 kg/m^3, and the heat flux reduces stratification by 0.11 kg/m^3 (Figure 10), with the median net reduction of stratification as 0.49 kg m^{-3}. Results based on the median values suggest that these buoyancy fluxes are responsible for roughly 35% of the reduction in stratification during downwelling-favorable storms (Figure 11).

Cross-shelf velocities during upwelling-favorable storms are strong at the surface and weak at depth (Figure 9b), which causes the salinity transports to be more important than heat fluxes to the change in stratification over the water column (Figure 9f). During these upwelling-favorable storms, the mean cross-shelf salt flux increases stratification by 0.14 kg/m^3, while the mean cross-shelf heat flux decreases stratification by 0.02 kg/m^3 (Figure 10). The mean buoyancy fluxes act to increase stratification in the water column; however, the net impact of upwelling-favorable storms reduces stratification on average by 0.09 kg/m^3. Median values for upwelling-favorable storms show that the cross-shelf salt flux increases stratification by 0.04 kg/m^3. The cross-shelf heat flux does not change stratification, and the net reduction in stratification is only 0.03 kg/m^3. Using either mean or median values, the cross-shelf salt flux during upwelling-favorable winds is highly important in suppressing the overall reduction in stratification (Figure 11).

The buoyancy fluxes discussed above highlight that downwelling-favorable winds are more effective at reducing stratification than winds in the opposite direction. Mean buoyancy fluxes are responsible for a difference of 0.45 kg/m^3 between the opposing wind directions in terms of impacting the stratification, while calculations using median values still result in a 0.23 kg/m^3 difference (Figure 11). Overall, cross-shelf advective fluxes of both salinity and potential temperature (Figure 10) are an important mechanism for changing the stratification during storms. Advective processes can be reversed; however, we have shown that within this shelf system, storm-induced destratification remains after the storm and thus these processes are important to the overall shelf destratification (Figure 4).

The New Jersey shelf maintains strong cross-shelf salinity gradients throughout the year due to river output along the coast (Manning, 1991). Within the New Jersey shelf system, the strong cross-shelf salinity gradients allow for large changes of stratification due to an Ekman buoyancy flux during storms. This is in contrast to L03 on the New England Shelf where the cross-shelf salinity gradients are significantly weaker as there is less river outflow in that region and as such L03 only focused on changes to the thermal stratification during fall. The

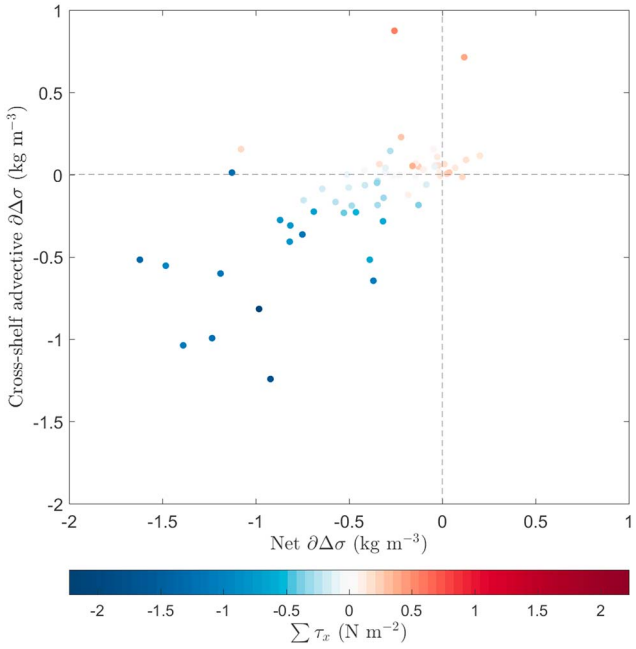

Figure 11. The net change in stratification (delta sigma) versus the cross-shelf advective impact on stratification for each storm. The color is the accumulated along-shelf wind stress (sum of the along-shelf wind stress for the duration of the storm) for the storm.

spatial distribution of salinity is thus important in determining how stratification is broken down in different coastal regions. Furthermore, the along-shelf direction on the New England shelf is east and west but the along-shelf direction off the coast of New Jersey is northeast to southwest. A downwelling-favorable storm over New Jersey may not be downwelling favorable south of Cape Cod. Because of the along-shelf variations, the breakdown of stratification on the MAB shelf is likely not coherent and would require further study to examine the spatial variability.

4.2. Enhanced Shear

Another mechanism contributing to the dependence of the erosion of stratification on wind direction is an increase in velocity shear during downwelling-favorable winds which was also found in L03. This enhanced shear was proposed to potentially be a result of an enhanced cross-shelf density gradient, leading to enhanced along-shelf thermal-wind shear. Calculating the average along-shelf geostrophic velocities during storms of both along-shelf wind directions, and referencing the velocities to the bottom, shows only a very weak enhanced surface to bottom shear for downwelling-favorable winds (Figure 12). The enhanced shear due to the changing thermal-wind shear is not enough to explain the overall increased shear.

While the mechanism that leads to the enhanced shear in the model output is not clear, we can nevertheless calculate the Richardson number ($R_g = \frac{g\Delta\rho\Delta z}{\rho_0(\Delta u^2+\Delta v^2)}$) during the storms to see if the enhanced shear meets the conditions for shear instabilities more often during downwelling-favorable storms, thus allowing a greater reduction in stratification. We calculate the Richardson number at each time interval during storms and then calculate the fraction of time during storms that the Richardson number is less than 0.25, a necessary but not sufficient condition for shear instabilities (Price et al., 1986). In the top 30 m, both upwelling favorable and downwelling favorable storms meet the criterion necessary for shear instabilities an equal fraction of the time (Figure 13). However, below 30 m, downwelling-favorable storms meet the conditions for shear instabilities a greater fraction of the time than do upwelling-favorable winds. Instabilities and mixing at depth could be an important driver for the breakdown in stratification due to the presence of the cold pool. The added ability for downwelling-favorable winds to mix in the cold pool likely enables a greater reduction in stratification relative to upwelling-favorable winds.

5. Tropical Storm Ernesto

Comparing the model output with observations from Tropical Storm Ernesto in 2006 suggests that the processes that reduce stratification described above, which are based on the model output are consistent with observations. Comparisons of the winds from the model and data confirm that the along-shelf winds are

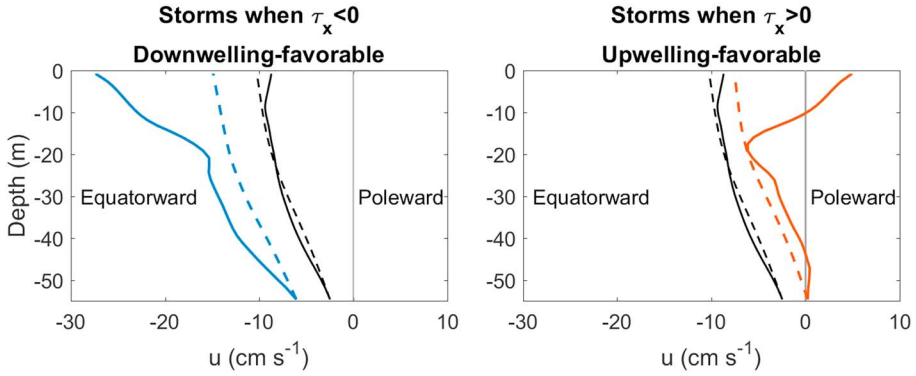

Figure 12. Mean along-shelf velocity (colored solid lines) and velocity profiles calculating from mean thermal-wind shear (colored dashed lines) during downwelling-favorable winds and upwelling-favorable winds. Black lines represent the background mean velocities during fall.

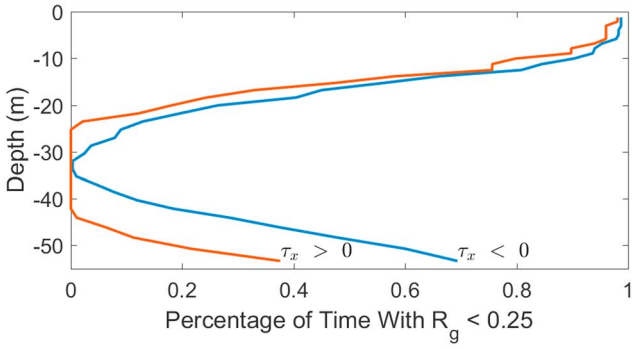

Figure 13. Fraction of time during strong wind events that the Richardson number was less than 0.25 at each depth. The blue line represents the downwelling-favorable winds, and the red line represents the upwelling-favorable winds.

downwelling favorable and that the forcing used in the model well represents the observed along-shelf winds (Figure 14). The cross-shelf winds reach similar magnitudes in the model and observations; however, they peak later within the storm in the model. Neither the direction nor the magnitude of the cross-shelf winds during storms was found to be significantly correlated to the change in stratification within the MABGOM model; thus, the accuracy with the along-shelf winds, which is more relevant to the stratification change, allows for further comparisons.

Within the model, the changes to the salinity, potential temperature, and potential density during Ernesto all act as expected from the above analysis for a downwelling-favorable storm. The salinity transects show the expected cross-shelf salinity gradients with fresher waters onshore (Figures 15a and 15c). Salinity increases at the surface and decreases near the bottom, reducing stratification (Figure 15e). Cross-shelf velocities during this storm (not shown here) acting on the cross-shelf salinity gradient lead to a buoyancy flux that reduces stratification.

Potential temperature fields within the model show weak cross-shelf thermal gradients at the surface and stronger gradients at depth with the cold pool onshore of this study location (Figures 16a and 16c). The overall changes to potential temperature show a universal cooling, with enhanced areas of cooling near the surface and at depth (Figure 16e). Strong cooling near the surface is due to the negative surface heat flux, and also wind-driven mixing into the thermocline. However, we also see that within the model, there is cooling at depth. This location is offshore of the cold pool, which means there are colder waters in the onshore direction close to the bottom. Thus, the offshore velocities at depth transport colder waters, which leads to the cooling here at depth.

The salinity transects from SW06 also show fresher waters onshore (Figures 15b and 15d). The changes in salinity compare well between the observations and the model on the furthest onshore edge of the transect with increasing salinity at the surface and decreasing salinity at depth (Figure 15f). This suggests that the cross-shelf salinity fluxes are important on the shelf. However, offshore of the 90-m isobath there is freshening during the storm throughout the water column. Before the storm, waters with 35.9 psu are observed offshore of the shelf indicating the presence of Gulf Stream/warm core ring water. After the storm, the salinities are significantly reduced offshore, likely due to the ring moving away from the shelfbreak via processes unrelated to the storm.

Potential temperature fields from the SW06 experiment are very similar to the model fields (Figures 16b and 16d). The observations show cooling throughout the water column, with much stronger cooling near the surface when compared to the model (Figure 16f). This difference in surface cooling can be partially attributed

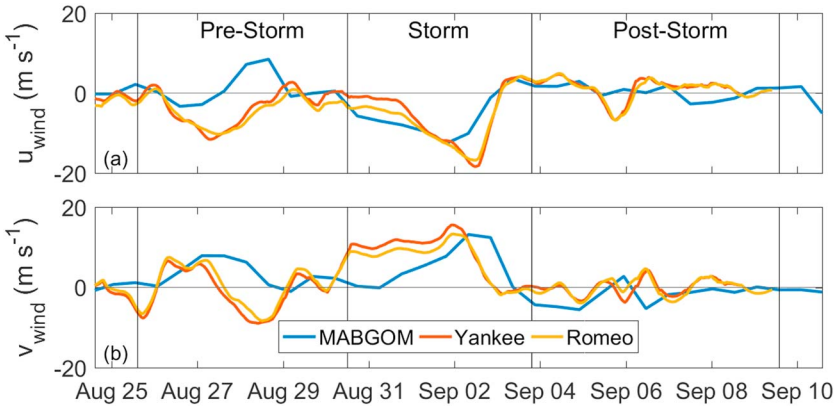

Figure 14. Comparing model wind forcing (blue) with the measured winds from the two Air-Sea Interaction Spar buoys Yankee (red) and Romeo (orange; positions of buoys in Figure 3). (a) Along-shelf winds on a 12-hr moving average and (b) cross-shelf winds on a 12-hr moving average. Vertical lines show the boundaries that define time periods before the storm, during the storm, and after the storm. MABGOM = Middle Atlantic Bight and Gulf of Maine.

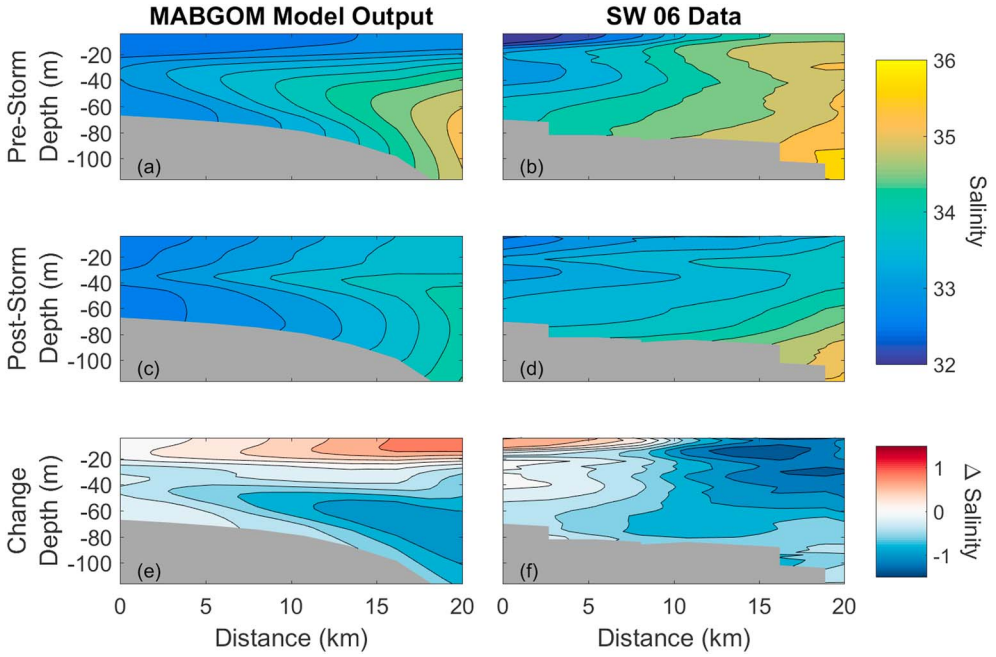

Figure 15. Comparison of salinity conditions associated with storms between the MABGOM model and the observations. The left column shows the MABGOM model output, and the right column shows the SW06 data. (a, b) The mean salinity fields for prestorm conditions. (c, d) The mean salinity fields for poststorm conditions. (e, f) The change from the prestorm to the poststorm (positive values indicate an increase in salinity). MABGOM = Middle Atlantic Bight and Gulf of Maine; SW06 = Shallow Water '06.

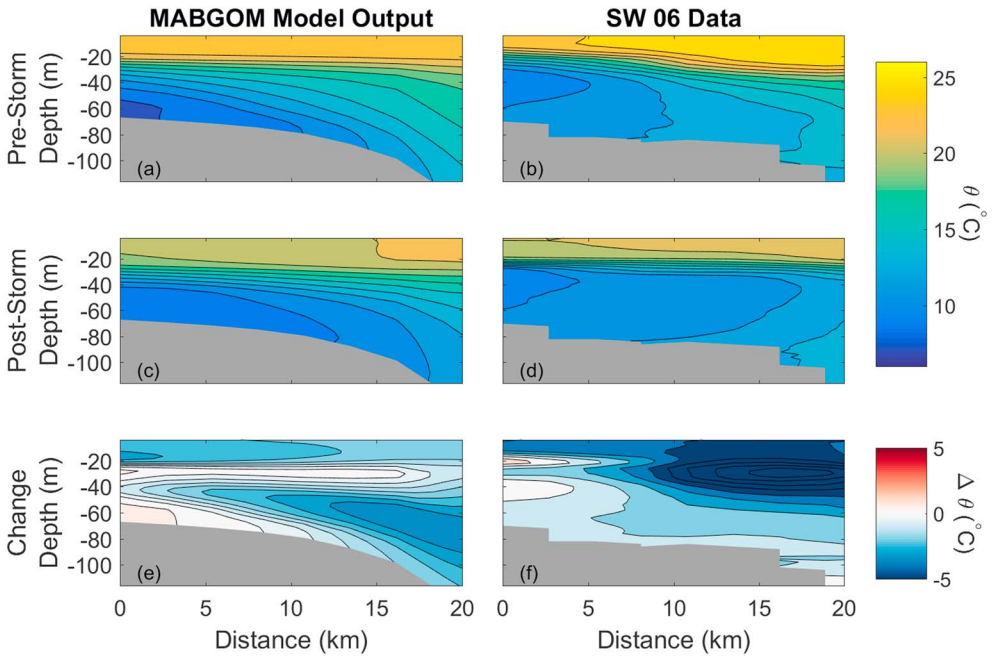

Figure 16. As in Figure 15 but with potential temperature (θ). MABGOM = Middle Atlantic Bight and Gulf of Maine; SW06 = Shallow Water '06.

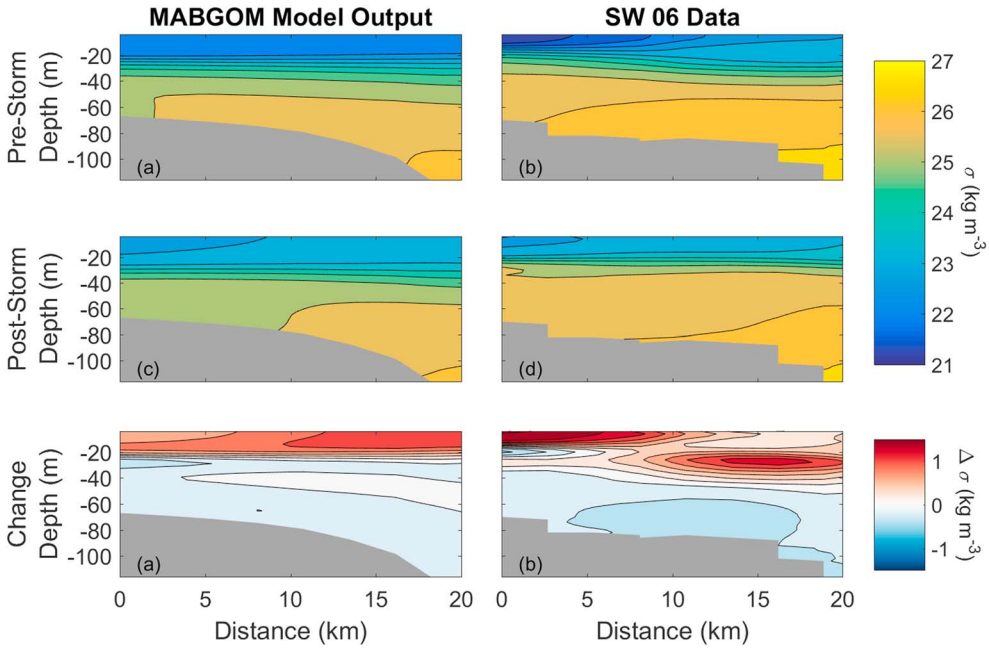

Figure 17. As in Figure 15 but with potential density (σ). MABGOM = Middle Atlantic Bight and Gulf of Maine; SW06 = Shallow Water '06.

to the difference in surface temperatures between the model and observations as the observations are found to be much warmer initially at the surface. The cooling at depth could be attributed to the offshore transport of cold pool waters, once again suggesting that buoyancy fluxes are important during storms.

Overall, both the model and observations show qualitatively the expected changes to potential density for a downwelling-favorable storm, which is an increase of density at the surface, and a decrease at depth leading to a reduction in stratification (Figure 17). The increase in density at the surface is due to the negative surface heat fluxes, and also the increasing salinity on the shelf. Near the bottom on the shelf, there was a decrease in salinity and a decrease in potential temperature. The changes to the potential density show that both the model and observations have a decrease in potential density at depth, indicating that the decrease in salinity had a larger impact on potential density than the decrease in potential temperature. This further emphasizes that changes to salinity are important in understanding how stratification changes on the shelf off of New Jersey, where the cross-shelf salinity gradients are large due to the presence of the Hudson River discharge.

6. Conclusions

Analysis of 10 years of the modeled seasonal evolution of stratification over the New Jersey shelf demonstrates large interannual variability in the initial fall stratification and the date at which stratification is broken down. The initial fall stratification in each year is not correlated to the end date of stratification, making predictability for the breakdown of stratification in a given year extremely difficult without knowledge of the wind and buoyancy forcing. Comparing results from both a one-dimensional mixing model and a three-dimensional regional circulation model shows that surface heat fluxes alone are often not as important as wind forcing in reducing stratification.

Storms are often one of the most important factors in reducing stratification in the fall. Downwelling-favorable winds are more effective at reducing stratification than upwelling-favorable winds through both an Ekman buoyancy flux and an enhanced velocity shear. The difference in the effectiveness between downwelling-favorable and upwelling-favorable winds in reducing stratification is largely due to the cross-shelf transport of salinity. Understanding the magnitude of the cross-shelf salinity gradients is important in informing how the stratification over the New Jersey shelf will break down during high wind events.

Model-data comparisons during Tropical Storm Ernesto show evidence that the model physics are qualitatively consistent with the observations. Changes in the salinity and temperature structures suggest that cross-shelf buoyancy fluxes are indeed important to the change in stratification on the shelf for a

downwelling-favorable storm. Further analysis with upwelling-favorable winds are needed to confirm the differential effects between storms in each along-shelf direction.

Knowing how stratification breaks down throughout the fall can aid in informing fisheries science and regulation, and storm forecasting. Cold pool temperatures in fall are directly impacted by changes to stratification, and these cold pool temperatures have been tied to the recruitment of species like yellowtail flounder (Sullivan et al., 2005). Tropical storm intensities have recently been found to be dependent on the cooling ahead of the eye of the storm, which is dependent on how much thermal stratification is broken down (Glenn et al., 2016). Maintaining measurements of not only the temperature structure but salinity structure is important to better understand and protect coastal communities.

Acknowledgments
J. S. T. F., M. A., and K. C. were supported by NSF grant OCE-1634094. K. C. was also partially supported by NSF grant OCE-1558960. G. G. was supported by CINAR via NOAA Cooperative Agreement NA13OAR4830233 and also the Iselin Chair for Senior Scientists at WHOI. Data used in this work are available at http://www.whoi.edu/page.do?pid=161917.

References

Beardsley, R. C., Chapman, D. C., Brink, K. H., Ramp, S. R., & Schlitz, R. (1985). The Nantucket Shoals Flux Experiment (NSFE79). Part I: A basic description of the current and temperature variability. *Journal of Physical Oceanography*, *15*(6), 713–748. https://doi.org/10.1175/1520-0485(1985)015<0713:TNSFEP>2.0.CO;2

Boicourt, W., & Hacker, P. (1976). Circulation on the Atlantic continental shelf of the United States, Cape May to Cape Hatteras. *Memoires de la Societe Royale des Sciences de Liege*, *6*, 187–200.

Chassignet, E. P., Hurlburt, H. E., Smedstad, O. M., Halliwell, G. R., Hogan, P. J., Wallcraft, A. J., et al. (2007). The HYCOM (HYbrid Coordinate Ocean Model) data assimilative system. *Journal of Marine Systems*, *65*(1–4), 60–83. https://doi.org/10.1016/j.jmarsys.2005.09.016

Chen, K., Gawarkiewicz, G. G., Lentz, S. J., & Bane, J. M. (2014). Diagnosing the warming of the Northeastern US Coastal Ocean in 2012: A linkage between the atmospheric jet stream variability and ocean response. *Journal of Geophysical Research: Oceans*, *119*, 218–227. https://doi.org/10.1002/2013JC009393

Chen, K., & He, R. (2015). Mean circulation in the coastal ocean off northeastern North America from a regional-scale ocean model. *Ocean Science*, *11*(4), 503–517. https://doi.org/10.5194/os-11-503-2015

Chen, K., He, R., Powell, B. S., Gawarkiewicz, G. G., Moore, A. M., & Arango, H. G. (2014). Data assimilative modeling investigation of Gulf Stream Warm Core Ring interaction with continental shelf and slope circulation. *Journal of Geophysical Research: Oceans*, *119*, 5968–5991. https://doi.org/10.1002/2014JC009898

Csanady, G. T. (1982). *Circulation in the Coastal Ocean*. Dordrecht, Holland: D. Reidel Publishing Company.

Curry, R. (1996). *HYDROBASE: A database of hydrographic stations and tools for climatological analysis* (Technical Report WHOI-96-01). Woods Hole, MA: Woods Hole Oceanographic Institution.

Fairall, C. W., Bradley, E. F., Hare, J. E., Grachev, A. A., & Edson, J. B. (2003). Bulk parameterization of air sea fluxes: Updates and verification for the COARE algorithm. *Journal of Climate*, *16*(4), 571–591. https://doi.org/10.1175/1520-0442(2003)016<0571:BPOASF>2.0.CO;2

Flagg, C. N., Dunn, M., Wang, D.-P., Rossby, H. T., & Benway, R. L. (2006). A study of the currents of the outer shelf and upper slope from a decade of shipboard ADCP observations in the Middle Atlantic Bight. *Journal of Geophysical Research*, *111*, C06003. https://doi.org/10.1029/2005JC003116

Forsyth, J. S. T., Andres, M., & Gawarkiewicz, G. G. (2015). Recent accelerated warming of the continental shelf off New Jersey: Observations from the CMV Oleander expendable bathythermograph line. *Journal of Geophysical Research: Oceans*, *120*, 2370–2384. https://doi.org/10.1002/2014JC010516

Fratantoni, P. S., & Pickart, R. S. (2007). The western North Atlantic shelfbreak current system in summer. *Journal of Physical Oceanography*, *37*(10), 2509–2533. https://doi.org/10.1175/JPO3123.1

Friedland, K. D., & Hare, J. A. (2007). Long-term trends and regime shifts in sea surface temperature on the continental shelf of the northeast United States. *Continental Shelf Research*, *27*(18), 2313–2328. https://doi.org/10.1016/j.csr.2007.06.001

Gawarkiewicz, G., Brink, K. H., Bahr, F., Beardsley, R. C., Caruso, M., Lynch, J. F., & Chiu, C.-S. (2004). A large-amplitude meander of the shelfbreak front during summer south of New England: Observations from the Shelfbreak PRIMER experiment. *Journal of Geophysical Research*, *109*, C03006. https://doi.org/10.1029/2002JC001468

Glenn, S., Miles, T., Seroka, G., Xu, Y., Forney, R., Yu, F., et al. (2016). Stratified coastal ocean interactions with tropical cyclones. *Nature Communications*, *7*, 10887.

Haidvogel, D., Arango, H., Budgell, W., Cornuelle, B., Curchitser, E., Lorenzo, E. D., et al. (2008). Ocean forecasting in terrain-following coordinates: Formulation and skill assessment of the Regional Ocean Modeling System. *Journal of Computational Physics*, *227*(7), 3595–3624. https://doi.org/10.1016/j.jcp.2007.06.016

Halliwell, G. R. (2004). Evaluation of vertical coordinate and vertical mixing algorithms in the Hybrid-Coordinate Ocean Model (HYCOM). *Ocean Modelling*, *7*(3-4), 285–322.

Hare, J. A., Morrison, W. E., Nelson, M. W., Stachura, M. M., Teeters, E. J., Griffis, R. B., et al. (2016). A vulnerability assessment of fish and invertebrates to climate change on the northeast U.S. continental shelf. *PLOS ONE*, *11*(2), 1–30. https://doi.org/10.1371/journal.pone.0146756

Houghton, R. W., Schlitz, R., Beardsley, R. C., Butman, B., & Chamberlin, J. L. (1982). The Middle Atlantic Bight cold pool: Evolution of the temperature structure during summer 1979. *Journal of Physical Oceanography*, *12*(10), 1019–1029. https://doi.org/10.1175/1520-0485(1982)012<1019:TMABCP>2.0.CO;2

Large, W., & Pond, S. (1981). Open ocean momentum flux measurements in moderate to strong winds. *Journal of physical oceanography*, *11*(3), 324–336.

Lau, W. K. M., Shi, J. J., Tao, W. K., & Kim, K. M. (2016). What would happen to superstorm sandy under the influence of a substantially warmer Atlantic Ocean? *Geophysical Research Letters*, *43*, 802–811. https://doi.org/10.1002/2015GL067050

Lentz, S. J. (2017). Seasonal warming of the Middle Atlantic Bight cold pool. *Journal of Geophysical Research: Oceans*, *122*, 941–954. https://doi.org/10.1002/2016JC012201

Lentz, S., Shearman, K., Anderson, S., Plueddemann, A., & Edson, J. (2003). Evolution of stratification over the New England shelf during the Coastal Mixing and Optics study, August 1996–June 1997. *Journal of Geophysical Research*, *108*(C1), 3008. https://doi.org/10.1029/2001JC001121

Li, Y., Fratantoni, P. S., Chen, C., Hare, J. A., Sun, Y., Beardsley, R. C., & Ji, R. (2015). Spatio-temporal patterns of stratification on the Northwest Atlantic Shelf. *Progress in Oceanography*, *134*, 123–137. https://doi.org/10.1016/j.pocean.2015.01.003

Linder, C. A., & Gawarkiewicz, G. (1998). A climatology of the shelfbreak front in the Middle Atlantic Bight. *Journal of Geophysical Research*, *103*(C9), 18,405–18,423. https://doi.org/10.1029/98JC01438

Manning, J. (1991). Middle Atlantic Bight salinity: Interannual variability. *Continental Shelf Research*, *11*(2), 123–137. https://doi.org/10.1016/0278-4343(91)90058-E

Mellor, G. L., & Yamada, T. (1982). Development of a turbulence closure model for geophysical fluid problems. *Reviews of Geophysics*, *20*(4), 851–875. https://doi.org/10.1029/RG020i004p00851

Mills, K. E., Pershing, A. J., Brown, C. J., Chen, Y., Chiang, F.-S., Holland, D. S., et al. (2013). Fisheries management in a changing climate: Lessons from the 2012 ocean heat wave in the Northwest Atlantic. *Oceanography*, *26*(2), 191–195.

Mooers, C. N., Fernández-Partagás, J. J., & Price, J. F. (1976). *Meteorological Forcing Fields of the New York Bight: First Year's Progress Report* (Technology Report TR76-8, 151 pp.). Miami, FL: University of Miami

Paulson, C. A., & Simpson, J. J. (1977). Irradiance measurements in the upper ocean. *Journal of Physical Oceanography*, *7*(6), 952–956. https://doi.org/10.1175/1520-0485(1977)007<0952:IMITUO>2.0.CO;2

Pershing, A. J., Alexander, M. A., Hernandez, C. M., Kerr, L. A., Le Bris, A., Mills, K. E., et al. (2015). Slow adaptation in the face of rapid warming leads to collapse of the Gulf of Maine cod fishery. *Science*, *350*(6262), 809–812. https://doi.org/10.1126/science.aac9819

Price, J. F., Weller, R. A., & Pinkel, R. (1986). Diurnal cycling: Observations and models of the upper ocean response to diurnal heating, cooling, and wind mixing. *Journal of Geophysical Research*, *91*(C7), 8411–8427. https://doi.org/10.1029/JC091iC07p08411

Rheuban, J. E., Kavanaugh, M. T., & Doney, S. C. (2017). Implications of future northwest atlantic bottom temperatures on the American lobster (Homarus americanus) fishery. *Journal of Geophysical Research: Oceans*, *122*, 9387–9398. https://doi.org/10.1002/2017JC012949

Shchepetkin, A. F., & McWilliams, J. C. (2005). The regional oceanic modeling system (ROMS): A split-explicit, free-surface, topography-following-coordinate oceanic model, Ocean Modelling. *Ocean Modelling*, *9*(4), 347–404. https://doi.org/10.1016/j.ocemod.2004.08.002

Straneo, F., Kawase, M., & Pickart, R. S. (2002). Effects of wind on convection in strongly and weakly baroclinic flows with application to the Labrador Sea. *Journal of Physical Oceanography*, *32*(9), 2603–2618. https://doi.org/10.1175/1520-0485(2002)032<2603:EOWOCI>2.0.CO;2

Sullivan, M. C., Cowen, R. K., & Steves, B. P. (2005). Evidence for atmosphere-ocean forcing of yellowtail flounder (Limanda ferruginea) recruitment in the Middle Atlantic Bight. *Fisheries Oceanography*, *14*(5), 386–399. https://doi.org/10.1111/j.1365-2419.2005.00343.x

Tang, D., Moum, J. N., Lynch, J. F., Abbot, P., Chapman, R., Dahl, P. H., et al. (2007). Shallow Water'06: A joint acoustic propagation/nonlinear internal wave physics experiment. *Oceanography*, *20*(4), 156–167.